Analysis of the ductility dip cracking in the nickel-base alloy 617mod

A Eilers[1], J Nellesen[2], R Zielke[2] and W Tillmann[1]

[1]Institute of Materials Engineering, TU Dortmund, Leonhard-Euler-Str. 2, 44227 Dortmund, Germany
[2]RIF e.V., Dortmund, Germany

Abstract. While testing steam leading power plant components made of the nickel-base alloy A617mod at elevated temperatures (700 °C), ductility dip cracking (DDC) was observed in welding seams and their surroundings. In order to clarify the mechanism of crack formation, investigations were carried out on welded specimens made of A617mod. Interrupted tensile tests were performed on tensile specimens taken from the area of the welding seam. To simulate the conditions, the tensile tests were conducted at a temperature of 700 °C and with a low strain rate. Local strain fields at grain boundaries and inside single grains were determined at different deformation states by means of two-dimensional digital image correlation (DIC). Besides the strain fields, local hardnesses (nanoindentation), energy dispersive X-Ray spectroscopy (EDX), and electron backscatter diffraction (EBSD) measurements were performed. Besides information concerning the grain orientation, the EBSD measurement provides information on the coincidence site lattice (CSL) at grain boundaries as well as the Schmid factor of single grains. All results of the analysis methods mentioned above were correlated and compared to each other and related to the crack formation. Among other things, correlations between strain fields and Schmid factors were determined. The investigations show that the following influences affect the crack formation: orientation of the grain boundaries to the direction of the loading, the orientation of the grains to each other (CSL), and grain boundary sliding.

1. Introduction

The nickel-base alloy 617mod is planned to be used for steam leading pipes in power plants with steam temperatures of 700 °C. In a test run under operation conditions at an elevated temperature of 700 °C ductility dip cracking (DDC) occurred in the area of the welding seam [1-3].

DDC occurs in nickel-base alloys and austenitic steels during solidification or reheating (i.e. during the welding process). The ductility of these materials shows a sharp drop at temperatures above approximately half the melting temperature. DDC is described as a grain boundary sliding, creep-like phenomenon. The grain boundary sliding (mainly at 45° to stress direction) leads to higher strain concentrations at triple points and other irregularities, where a grain boundary changes its direction. The high strains result in micro-voids leading to intergranular crack formation [4-6].

In this study, investigations regarding the mechanism of crack formation in the welded area of the alloy 617mod were carried out. Tensile specimens were taken from a welded pipe and deformed in interrupted tensile tests at an elevated temperature of 700 °C. The strain distribution at the specimen surface were determined using scanning electron microscopy (SEM) images and by means of digital image correlation (DIC) after every stage of the interrupted tensile test. The strain fields at grain boundaries and in single grains could be analysed due to the high resolution of the SEM images.

Besides the strain fields, the grain orientation (electron backscatter diffraction), the hardness (nanoindentation), and the Schmid factor were determined and compared to each other.

2. Experimental methods

2.1 Sample manufacturing and preparation

The tensile specimens were cut from a welded pipe segment made of the alloy 617mod using electrical discharge machining. The specimen gauge (length 5 mm, width 2 mm, thickness 1.85 mm) consists in equal parts of the welding seam and the base material (figure 1 left) so that during tensile testing both sections were loaded.

The grain orientations of the specimen gauge were observed by means of electron backscatter diffraction (EBSD) after polishing. The grain orientation is shown in figure 1 (right) with the Miller indices. Furthermore, the coincidence site lattices (CSL) were determined with the help of EBSD measurements. The CSL describes the orientation of the grains to one another using the Σ value [7, 8]. By specifying the stress direction and with the knowledge of the grain orientation, the Schmid factor could be determined, giving information about the orientation of the slip planes and slip directions.

After the EBSD measurements, titanium dots (diameter: approx. 2 µm, distance: 5 µm, thickness: 50 nm) were applied on the surface of the specimen by using photolithography and sputtering. These titanium dots (figure 2 left) created grey-scaled edges which were used for the SEM-based DIC to calculate the strain fields.

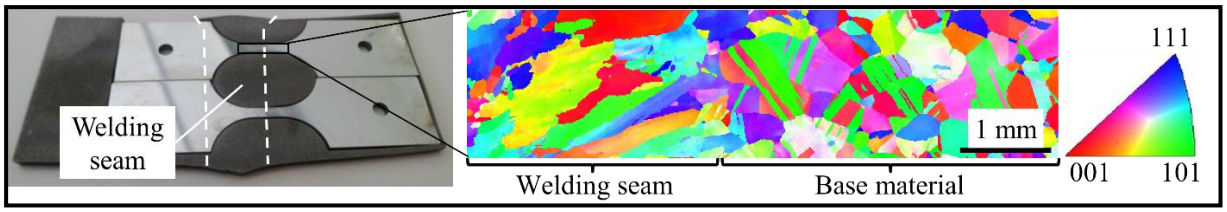

Figure 1. Left: Position of the two polished samples in a welded area (between the dashed lines) of a pipe segment; right: Grain orientation map with colour scale (Miller indices).

2.2 Selection of areas for the DIC in reference condition

The strain fields were determined with the help of the digital image correlation based on SEM images. A single image was magnified 650 times (image size approx. 190 x 140 µm). In order to cover a larger area with the images, nine single images were assembled to one image with a size of approx. 500 x 400 µm. Three of these assembled areas were selected for each specimen (figure 2 right).

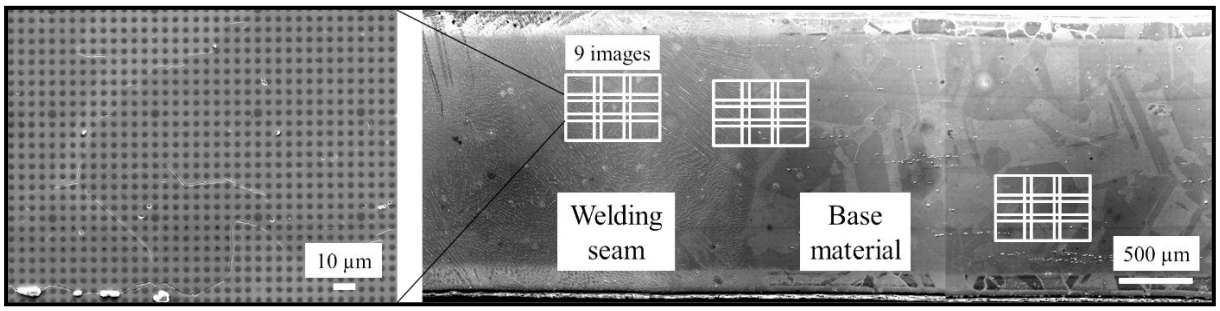

Figure 2. Left: Titanium dots (diameter: approx. 2 µm, distance: 5 µm, thickness: 50 nm) on the specimen surface used for the DIC; right: Gauge section with three areas (nine images each).

2.3 Interrupted tensile test
After the preparation, EBSD measurements, and taking SEM images the specimens were inserted into the experimental setup. The specimens were deformed at an elevated temperature of 700 °C in several stages. After every stage, the specimens were cooled down, removed from the setup, and SEM images were taken of the same areas as in the reference condition. The experiments were conducted with the test machine RMK 100 (Schenk) using a deformation speed of 3.2 µm/min ($\dot{\varepsilon} = 10^{-5}$ s^{-1}).

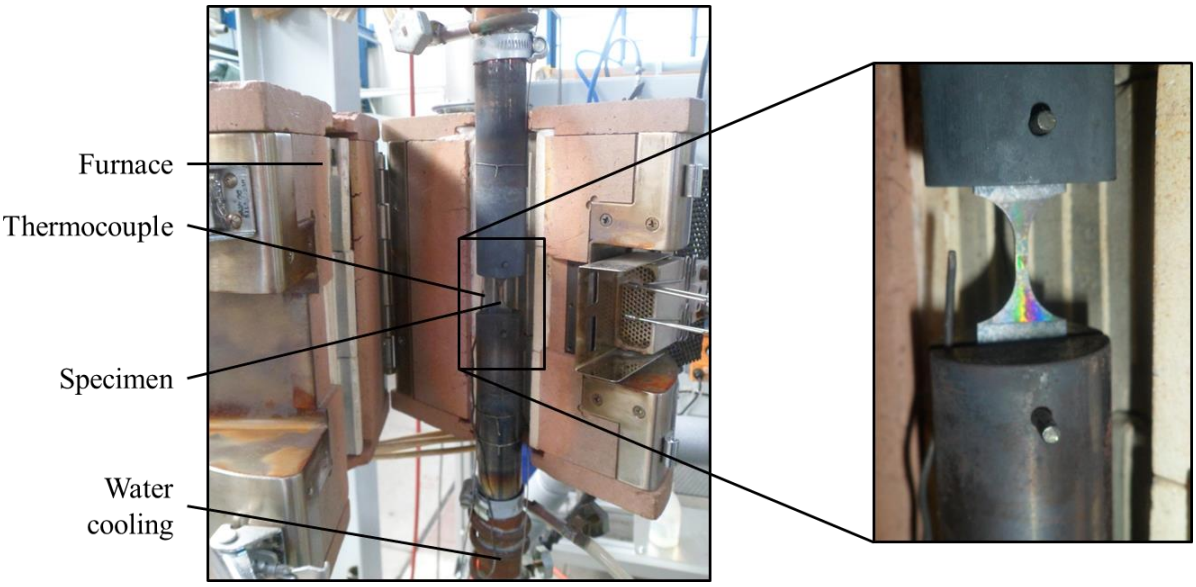

Figure 3. Experimental setup of the tensile test at 700 °C.

2.4 Digital image correlation (DIC)
SEM images in different deformation stages were generated of the same areas as in the reference condition after the interrupted tensile test (see 2.2.). The strain fields were calculated for every SEM image with the help of the DIC. The software used for the calculations was developed by the institute. The reference image and the deformed image were locally mapped to each other. Based on this local mapping a strain tensor was determined, that was used to calculate the scalar equivalent strain ε_{equ}.

2.5 Nanoindentation
After the tensile tests, the oxide layer, which was formed at the surface during these tests, were grinded off and hardness tests were carried out at room temperature by means of nanoindentation with a Nanoindenter G200 (Agilent). The depth of the indents was 500 nm and the distance between the indents was 20 µm. To evaluate if the hardness near the grain boundary deviates from the hardness inside the grains, measurements were conducted at grain boundaries showing DDC. Additionally, the hardness at grain boundaries without DDC was compared to the previous results.

3. Results and discussion
In the following different influences on DDC are described. The influence of the precipitate condition plays an important role [1, 6], but is not a subject of this investigation and will be focused on in future investigations.

3.1 Influence of the stress direction and grain boundary sliding on DDC
The SEM images of different deformation stages were at first visually investigated for cracks. Figure 4a shows a representative grain where DDC occurred. As shown in other investigations, the mechanism of DDC is related to grain boundary sliding [6]. Because of the maximum shear stress at

angles of 45° to the stress direction (cf. Schmid´s law), grain boundary sliding mainly occurs at these angles. If a sliding grain boundary changes its direction to higher angles (i.e. 90° to the stress direction), DDC occurs as a result of a higher strain concentration [6].

The above mentioned influence of the stress direction on grain boundary sliding and DDC was also observed in this work. Figure 4a shows the mechanism of grain boundary sliding at grain boundaries that are orientated 45 degrees in respect to the loading direction and DDC at higher angles. Grain boundary sliding could be proven and illustrated with the help of the strain distribution (figure 4b). The strain value is increased along the grain boundary with the highest values at the triple point where DDC will develop in further processes of deformation. Furthermore, the titanium dots are shifted along the grain boundary as visible in the SEM image.

Figure 5a shows a SEM image of the entire specimen gauge. It can be seen that DDC occurs in the welding seam as well as in the base material. The cracked grain boundaries are orientated at higher angles (45° to 90°) to the stress direction.

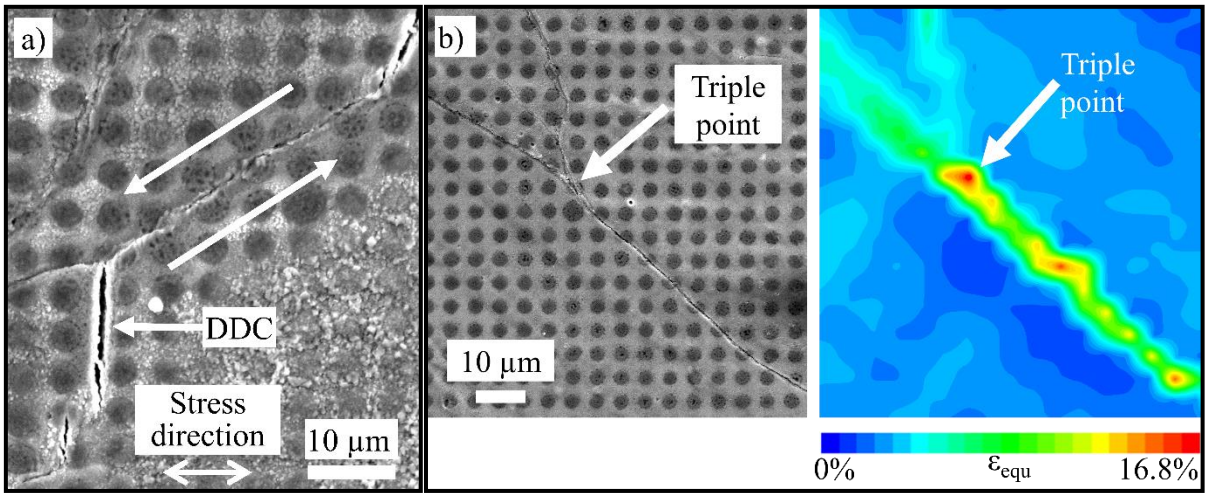

Figure 4. a) SEM image of sliding grain boundary (45° to stress direction) and resulting DDC (often 90° to stress direction); b) SEM image (left) and strain field (right) of a grain boundary (45° to stress direction) in the welding seam after the third deformation stage.

3.2 Influence of CSL on DDC

The CSL describes the orientation of the grains to each other. Figure 5b shows the grain boundaries of the specimen gauge. The Σ3 grain boundaries (red lines) are usually twin boundaries which have a lower grain boundary energy and therefore are more resistant to damages such as cracking and creep [7, 9]. The black lines indicate random grain boundaries divided in low angle (LAGB) and high angle grain boundaries (HAGB). A large number of twin boundaries (parallel red lines) are visible in the base material, while almost no red lines were detected in the welding seam.

The ductility dip cracks, which can be seen in figure 5a, are also marked in figure 5b. Almost all grain boundaries where DDC occurs, are random high angle grain boundaries (bold black lines) with a high angle to the stress direction (see 3.1). Many short cracks occur in the welding seam at wound grain boundaries with a lot of direction changes. These direction changes, along with the grain boundary sliding and the small number of Σ3 grain boundaries in the welding seam, explain the high number of cracks in these areas.

In order to verify that Σ3 grain boundaries are more resistant to DDC, local strain fields were investigated. Figure 6 shows a SEM Image (a), a SEM image with the CSL grain boundaries (b), and the strain field (c) of the same area. Figure 6b shows that a Σ3 grain boundary and a HAGB have the same (high) angle to the stress direction. The SEM image (a) as well as the strain field (b) show that deformation (and DDC) only occur at the HAGB (black line). The parallel Σ3 grain boundary (red

line) as well as the inside of the grain show no conspicuous deformation. These observations, together with the observations in figure 5b, confirm the assumption that Σ3 grain boundaries are more resistant to DDC than HAGB.

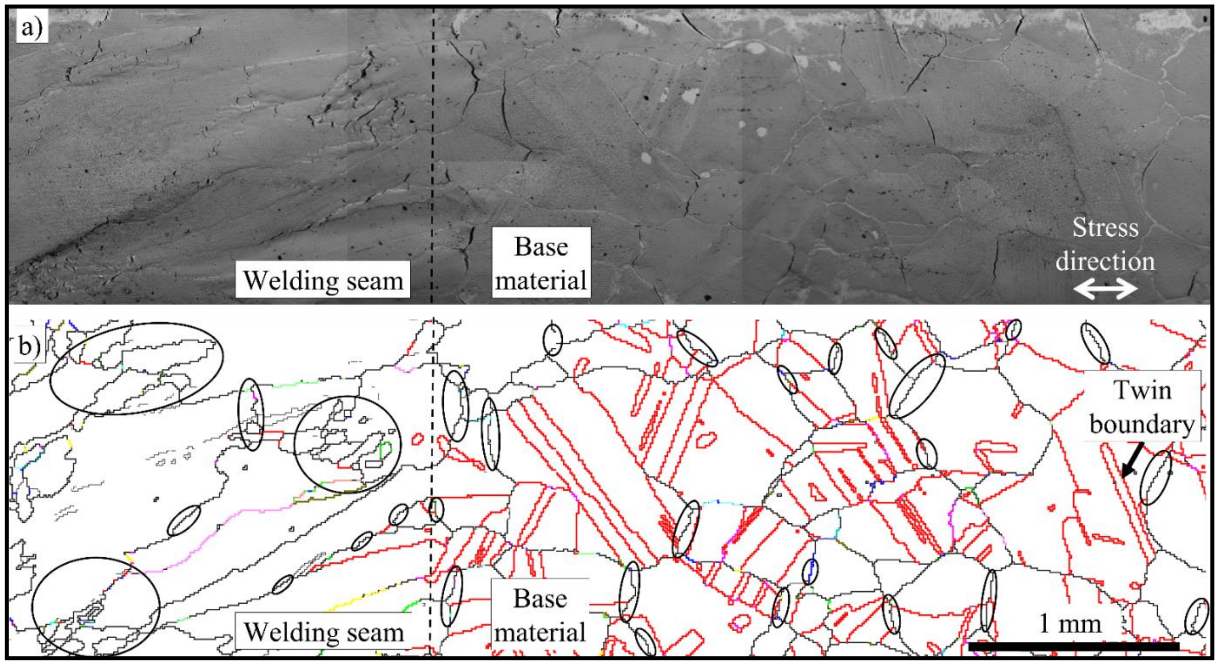

Figure 5. a) SEM image of the A617mod specimen after the sixth deformation stage with a large number of ductility dip cracks; b) grain boundaries of the same specimen: Red: Σ3 grain boundaries (CSL); coloured: Remaining CSL (Σ5 - Σ49); black (thin): Low angle grain boundaries (LAGB); black (bold): High angle grain boundaries (HAGB). The cracked grain boundaries are marked.

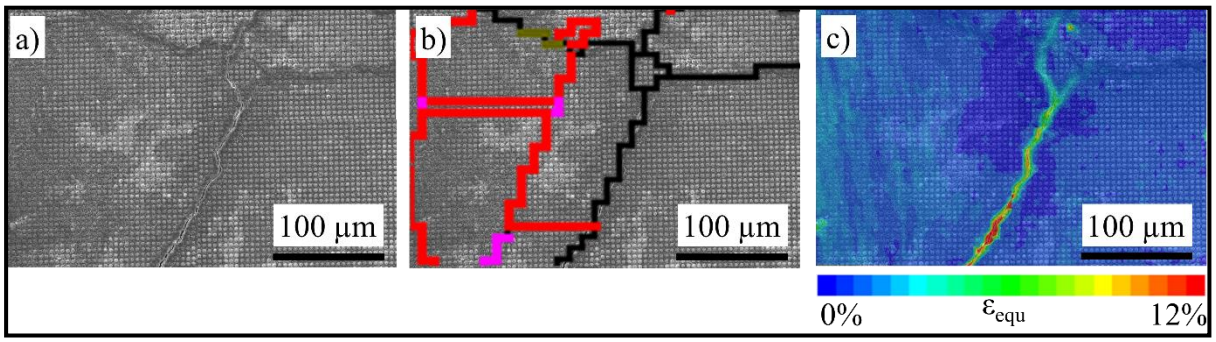

Figure 6. DDC in the base material of the A617mod after the third deformation stage: a) SEM image; b) grain boundaries (black: HAGB; red: Σ3 grain boundary; pink: Σ9 grain boundary; green: Σ25 grain boundary); c) strain field.

3.3 Influence of the hardness

As mentioned above (see 2.5.), hardness measurements were conducted in different areas of the specimen. All average values of the nanoindentation hardness measurements are between 5 and 5.5 GPa. No significant influence of the observed areas could be identified. This includes areas of grain boundaries with and without DDC as well as the inside of grains. In figure 7 an area in the welding seam with cracked grain boundaries is shown. The average hardness value is 5.46 GPa and the standard deviation is 0.46 GPa. For future investigations, hardness measurements at elevated temperatures are planned.

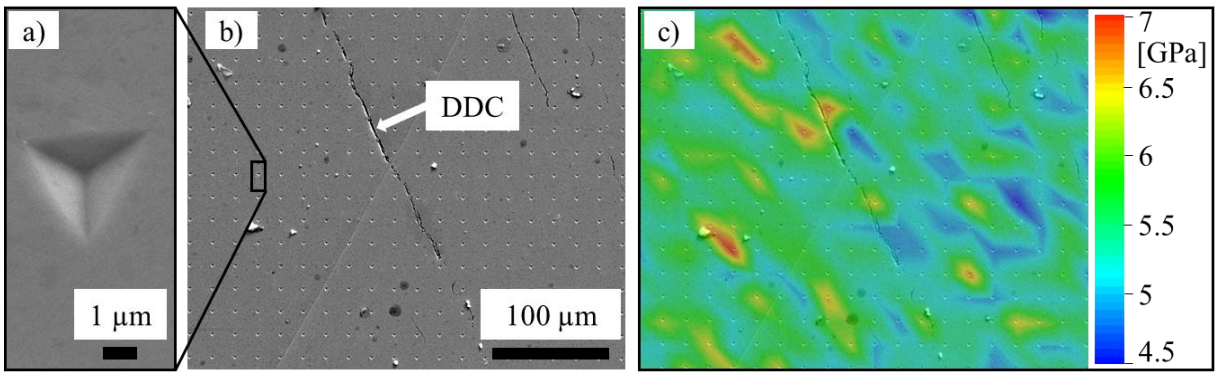

Figure 7. a) SEM image of a single indent; b) SEM image of an area with indents and DDC; c) SEM image of the same area with overlaid hardness values in [GPa].

3.4 Influence of the Schmid factor on the deformation within the grains

With the information of grain orientation and the stress direction, the Schmid factors were determined for every single grain using the software Channel 5 (Oxford). Nickel has a face centred cubic (fcc) crystal system. Thus, the slip systems with slip planes {111} and slip directions $[\bar{1}10]$ were selected. The higher the Schmid factor the higher the shear stresses are inside of the grains in the selected slip systems. The highest value (0.5) occurs for an angle of 45° to the stress direction [10]. If the critical resolved shear stress (CRSS) is reached, dislocation motion and, therefore, plastic deformation occurs. These deformations were proven with help of the strain field at grains with a higher Schmid factor (figure 8). The grain with a high Schmid factor (white) shows higher strain values with an angle of 45° to the stress direction. The grain with a low Schmid factor (black) shows no high strain values.

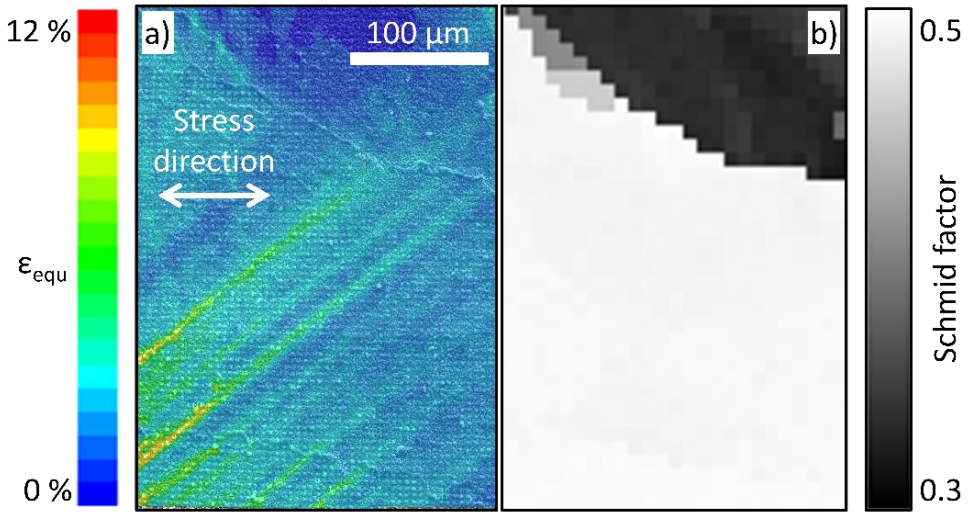

Figure 8. a) SEM image with overlaid strain field; b) Schmid factor of the same area.

4. Summary

Within the scope of this work, the welded nickel base alloy 617mod was investigated with interrupted tensile tests at an elevated temperature of 700 °C. Due to this thermomechanical stress DDC occurred. By means of DIC local strain fields were calculated. The grain orientation, CSL, and the Schmid factor were determined with the help of the EBSD. Furthermore, local hardness measurements were performed using nanoindentation.

DDC occurred at grain boundaries with a high angle (45° to 90°) to the stress direction. Grain boundary sliding appeared at grain boundaries with an angle of approx. 45° to the stress direction, leading to DDC in the further course of the grain boundary. The grain boundary sliding was proven with help of the strain field. Furthermore, it was shown that the orientation of the grains to each other (CSL) has an influence on DDC. Σ3 grain boundaries are more resistant to DDC than other grain boundaries.

Besides DDC, plastic deformation occurs especially in grains with a high Schmid factor, which could be proven with the help of the strain fields. Further investigations address the precipitate condition at the grain boundaries as well as heat treatments, that influence the precipitate condition. Additionally, hardness measurements at elevated temperatures are planned to determine the material behaviour during the formation of DDC.

Acknowledgments
The authors thank the "Deutsche Forschungsgemeinschaft" (DFG) for its financial support within the scope of the project TI 343 / 43-1.

References
[1] Ullrich C, Gierschner G, Stolzenberger C and Tschaffon H 2011 Erfahrungen beim Testbetrieb von Komponenten für das 700 °C Kraftwerk *VDI Wissensforum*
[2] Kuhn B, Ullrich C, Tschaffon H, Beck T and Singheiser L 2013 Stress-relaxation cracking test for welded joints *J. Test. Eval.* **41** 207–16
[3] Van Wortel H 2007 Control of relaxation cracking in austenitic high temperature components *Nace Corrosion Conference*
[4] Lippold J 2005 Recent developments in weldability testing for advanced materials *Joining of Advanced and Specialty Materials* **VII** 1–7
[5] Jang A Y, Lee D J, Shim J H, Kang S W and Lee H W 2011 Effect of Cr/Ni equivalent ratio on ductility-dip cracking in AISI 316L weld metals *Mater. Design* **32** 371–6
[6] Ramirez A J and Lippold J C 2004 High temperature behavior of Ni-base weld metal: Part II – Insight into the mechanism for ductility dip cracking *Mater. Sci. Eng. A* **380** 245–58
[7] Wen X 2014 Creep Behavior of high temperature alloys for generation IV nuclear energy systems *PhD Thesis* University of Cincinnati
[8] Föll H Defects in crystals *Hyperscript Christian-Albrechts-Universität Kiel* http://www.tf.uni-kiel.de/matwis/amat/def_en/index.html
[9] Gertsman V Y and Bruemmer S M 2001 Study of grain boundary character along intergranular stress corrosion crack paths in austenitic alloys *Acta Mater.* **49** 1589–98
[10] Roesler J, Harders H and Baeker M 2007 *Mechanical Behaviour of Engineering Materials: Metals, Ceramics, Polymers, and Composites* (Berlin: Springer) pp 180–182